Journal of Theoretical Biology 575 (2023) 111631

Contents lists available at ScienceDirect

Journal of Theoretical Biology

journal homepage: www.elsevier.com/locate/yjtbi

A mathematical model for nutrient-limited uniaxial growth of a compressible tissue

K. Li *, A.J. Gallo, B.J. Binder, J.E.F. Green

School of Computer and Mathematical Sciences, University of Adelaide, Adelaide, SA 5005, Australia

ARTICLE INFO

Keywords:
Uniaxial growth
Non-uniform growth
Reaction–diffusion
Yeast

ABSTRACT

We consider the uniaxial growth of a tissue or colony of cells, where a nutrient (or some other chemical) required for cell proliferation is supplied at one end, and is consumed by the cells. An example would be the growth of a cylindrical yeast colony in the experiments described by Vulin et al. (2014). We develop a reaction–diffusion model of this scenario which couples nutrient concentration and cell density on a growing domain. A novel element of our model is that the tissue is assumed to be compressible. We define replicative regions, where cells have sufficient nutrient to proliferate, and quiescent regions, where the nutrient level is insufficient for this to occur. We also define pathlines, which allow us to track individual cell paths within the tissue. We begin our investigation of the model by considering an incompressible tissue where cell density is constant before exploring the solution space of the full compressible model. In a large part of the parameter space, the incompressible and compressible models give qualitatively similar results for both the nutrient concentration and cell pathlines, with the key distinction being the variation in density in the compressible case. In particular, the replicative region is located at the base of the tissue, where nutrient is supplied, and nutrient concentration decreases monotonically with distance from the nutrient source. However, for a highly-compressible tissue with small nutrient consumption rate, we observe a counter-intuitive scenario where the nutrient concentration is not necessarily monotonically decreasing, and there can be two replicative regions. For parameter values given in the paper by Vulin et al. (2014), the incompressible model slightly overestimates the colony length compared to experimental observations; this suggests the colony may be somewhat compressible. Both incompressible and compressible models predict that, for these parameter values, cell proliferation is ultimately confined to a small region close to the colony base.

1. Introduction

The study of one-dimensional models of growing tissues has a long history in mathematical biology, with applications including tumour growth, wound healing and pattern formation e.g., Maini et al. (2004), Crampin et al. (1999), Breward et al. (2002), Neville et al. (2006), Baker et al. (2010). Such simplification of the geometry of the tissue permits a focus on the fundamental mechanisms and key variables influencing tissue development, renders the models more tractable to mathematical analysis, and improves computational efficiency. In some cases, this simplification comes at the expense of realism, since tissue growth is generally a three-dimensional process. However, there are biological examples where growth is confined to one direction, making the one-dimensional approximation more reasonable. One example would be the work of Vulin et al. (2014), where cylindrical yeast colonies are grown in such a way that their expansion is confined to the axial direction.

Like all organisms, yeast requires a nutrient source such as glucose to grow and proliferate. In the experiments by Vulin et al. (2014), yeast was restricted to grow in the direction perpendicular to the surface of the Petri dish, with a fixed radius by controlling the nutrient supply at the base of the colony. By regulating the glucose delivery, Vulin et al. (2014) hypothesised that the colony experiences a monotonically decreasing nutrient gradient within the colony. It was then hypothesised that it is this non-constant nutrient gradient which causes the colony to have two regions of growth. A nutrient rich replicative region where cells are able to proliferate and a nutrient poor quiescent region where cells cannot proliferate (Fig. 1(a)).

Through their experimental design Vulin et al. (2014) observed a linear increase in the height of the cylindrical yeast colony over time (Fig. 1(b)). It was proposed by Vulin et al. (2014) that the linear growth of the colony length is the result of a limited nutrient supply that can only reach a certain point within the colony. We wish to validate

* Corresponding author.
E-mail address: kai.li02@adelaide.edu.au (K. Li).

https://doi.org/10.1016/j.jtbi.2023.111631
Received 31 May 2023; Received in revised form 16 August 2023; Accepted 1 October 2023
Available online 5 October 2023

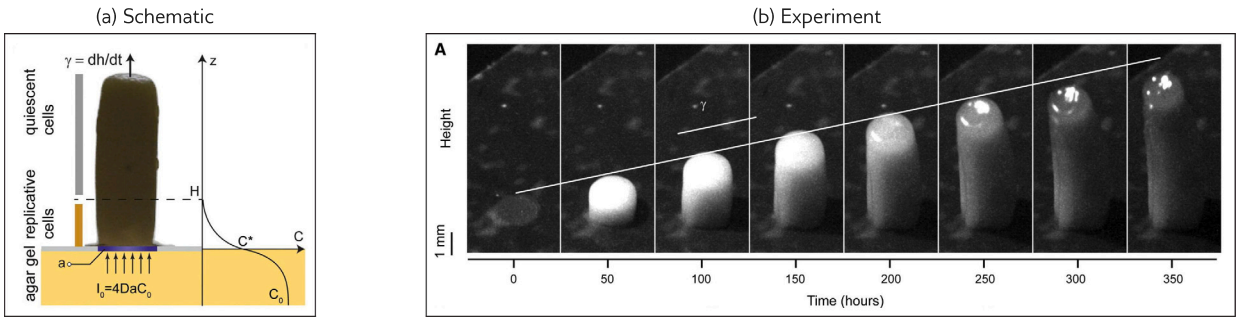

Fig. 1. **(a)** Schematic of uniaxial growth. Glucose is supplied at a constant rate at the base of the colony. However, the nutrient concentration, C can only travel a certain distance, H up the colony. The region below H is a replicative region where cells can proliferate and above H is a quiescent region where cells cannot proliferate. **(b)** Experimental image of cylindrical yeast colony showing the height or length, $L(t)$ to grow linearly over time.
Source: Modified images taken with permission from Vulin et al. (2014).

this hypothesis using a continuous partial differential equation (PDE) approach (Deroulers et al., 2009; Baker et al., 2010; Yates et al., 2012).

Previously, Gallo et al. (2021) proposed a discrete agent-based model coupled with a continuum approximation to predict the growth of uniaxial yeast colony. In their model, the nutrient was prescribed and fixed for all time. In addition, Vulin et al. (2014) used a simple PDE model to predict the evolution of the nutrient concentration (the resulting curve can be found in Fig. 1(a)). However, in both models there were limiting assumptions such as the nutrient concentration was not coupled with cell proliferation or assumed to be constant and the cells were also assumed to be incompressible. We wish to extend these previous works to model cell proliferation and nutrient transport as a coupled system. Additionally, we also relax the assumption that the tissue is incompressible.

In this paper, we present a PDE model for tissue growth consisting of reaction–advection–diffusion equations for the nutrient concentration and cell density, coupled with an constitutive equation relating the velocity field to the pressure gradient, and an equation of state relating the pressure to the cell density. The system is formulated as a free boundary problem, where the length of the growing tissue is determined as part of the solution process. Similar models for tissue growth have been developed previously, often motivated by application to tumour growth (Byrne and Chaplain, 1995; Chaplain, 1996; Painter, 2009; Hecht and Vauchelet, 2017). Note, as this work is motivated by uniaxial growth with application to cylindrical yeast colonies, we use the terms tissue, colony and domain interchangeably throughout this paper.

By linking nutrient concentration with cell density and colony length, we find that the length of the tissue or colony increases in proportion to time when there is a region of fixed length in which the cells have sufficient nutrient to proliferate, while all other cells remain inactive. This finding is consistent with experimental observations reported by Vulin et al. (2014). Furthermore, in the compressible model, we observe a counter-intuitive phenomenon. When the rate of nutrient consumption is small, the nutrient concentration is not always monotonically decreasing throughout the domain. This effect results from a combination of the compressibility of the tissue, and nutrient advection.

In addition to Vulin et al. (2014)'s cylindrical colony experiment, the system of coupled PDEs developed in this work can be readily applied to other biological systems exhibiting uniaxial growth. Binder et al. (2008), for example, showed that avian gut tissue growth can be modelled in one dimension. In their work, the authors used a piece-wise incompressible domain to model non-uniform proliferation. However, this is not entirely satisfactory as non-uniformity is likely to vary smoothly across the domain rather than suddenly or rapidly across the piece-wise regions of tissue. Modelling avian gut growth with the full PDE model described in our work would therefore allow for an investigation into non-uniform tissue proliferation with and without the effect of tissue compressibility. Other examples of uniaxial growth include bone growth (Czarnecki et al., 2014). In this example, cells would most likely experience compression, hence making our model highly applicable in this physical scenario.

The rest of this article is organised as follows. In Section 2, we present the mathematical model of the reaction–advection–diffusion system. In Section 3, we introduce pathlines and the distinction between replicative and quiescent regions. Furthermore, we devise a systematic method to differentiate between uniform, non-uniform, and no proliferation using pathlines, all while preserving our understanding of the global growth characteristics of the domain. In Section 4, we explore the simplified incompressible model and present the results from the numerical simulation. In Section 5, we examine the full compressible model and present additional results from the numerical simulation. Our model is then applied to the yeast experiments of Vulin et al. (2014) in Section 6. Lastly, we provide a summary and discussion of the main findings in Section 7.

2. Mathematical model

We consider a tissue or cell colony, the growth of which is restricted to one spatial dimension. We assume it occupies the region $0 \le x \le L(t)$, where t denotes time. The base of the tissue is assumed to be at $x = 0$, and $x = L(t)$ denotes the top of it. The tissue is assumed to contain live cells which are capable of proliferation. However, this process requires a nutrient, which is transported by a combination of advection and diffusion. The velocity field within the tissue arises as a result of cell proliferation, and leads to domain growth (Neville et al., 2006). We denote the cell density by $\rho(x,t)$, and nutrient concentration by $C(x,t)$.

We assume that the cells move by a combination of advection, with velocity $u(x,t)$, and diffusion, with coefficient D_ρ. The rate of cell proliferation is assumed to depend on the cell density, ρ, and nutrient concentration C within the colony. Hence, by conservation of mass we have:

$$\frac{\partial \rho}{\partial t} + \frac{\partial}{\partial x}(u\rho) = D_\rho \frac{\partial^2 \rho}{\partial x^2} + k\rho C, \tag{1}$$

where k a constant and $k\rho C$ is the rate of cell proliferation. Similarly, the nutrient is assumed to be transported by a combination of advection and diffusion (with coefficient D_C). We set the rate of nutrient consumption to be $\lambda\rho C$, where λ is a constant nutrient consumption rate. We thus obtain the following equation for C:

$$\frac{\partial C}{\partial t} + \frac{\partial}{\partial x}(uC) = D_C \frac{\partial^2 C}{\partial x^2} - \lambda\rho C. \tag{2}$$

In order to obtain an equation for the velocity u, we require a constitutive relation which specifies the mechanical properties of the system. We follow Byrne and Chaplain (1997) by using Darcy's Law which relates the velocity to the pressure, P, by:

$$u = -\alpha \frac{\partial P}{\partial x}, \tag{3}$$

where α is a constant. We also require an equation of state that relates the pressure to the cell density, $\rho(x,t)$. For simplicity, we choose the linear relationship

$$P = \frac{\rho - \rho_0}{\beta}, \tag{4}$$

where ρ_0 is the cell density when the cells are not compressed and β is a compressibility constant. The system is incompressible in the limit $\beta \to 0$. Hence, we note that the pressure law is singular in the incompressible limit. We consider this limit further in Section 4.

Finally, we require an equation for $L(t)$. Following Neville et al. (2006), we assume that the material at the top of the tissue moves with the local cell velocity, which we denote by $v(x,t)$. This velocity is, in turn, related to the cell flux, J_ρ by

$$J_\rho = \rho u - D_\rho \frac{\partial \rho}{\partial x} = \rho v,$$

so

$$\frac{dL}{dt} = v|_{x=L(t)} = \left[u - \frac{D_\rho}{\rho}\frac{\partial \rho}{\partial x}\right]\Big|_{x=L(t)}. \tag{5}$$

To track the position of cells within the domain we employ pathlines which are given by

$$\frac{dX}{dt} = v|_{x=X(t)} = \left[u - \frac{D_\rho}{\rho}\frac{\partial \rho}{\partial x}\right]\Big|_{x=X(t)}. \tag{6}$$

To close our system of model equations, we now specify the necessary boundary and initial conditions. Firstly, the velocity at the base of the tissue is zero and thus

$$u|_{x=0} = 0. \tag{7}$$

Then, from Eq. (3) we see that this implies:

$$\frac{\partial P}{\partial x}\Big|_{x=0} = 0. \tag{8}$$

We assume continuity of pressure across the tissue boundary, so at the top of the tissue, the pressure will be atmospheric pressure. However, since pressure is only unique up to an additive constant, we set the zero of the pressure scale to be atmosphere pressure, so that

$$P|_{x=L(t)} = 0. \tag{9}$$

Eq. (9) can be generalised in varies ways e.g., by including the effects of surface tension. For simplicity, we neglect such additional effects here and just impose continuity of pressure. We assume also that nutrient is supplied at the base of the tissue at a constant concentration, $C|_{x=0} = C_0$, and that there is no flux of nutrient out of the tissue at the top, so

$$\frac{\partial C}{\partial x}\Big|_{x=L(t)} = 0. \tag{10}$$

We assume the initial tissue length is $L(0) = L_0$. At $t = 0$, the nutrient is assumed to be present only at the base of the tissue, and hence we impose the initial condition

$$C|_{t=0} = C_I(x) = \begin{cases} C_0 & \text{if } x = 0, \\ 0 & 0 < x \le L_0. \end{cases}$$

Thus, in summary, our system of model equations is:

$$\frac{\partial C}{\partial t} + \frac{\partial}{\partial x}(uC) = D_C \frac{\partial^2 C}{\partial x^2} - \lambda \rho C, \tag{11a}$$

$$\frac{\partial \rho}{\partial t} + \frac{\partial}{\partial x}(u\rho) = D_\rho \frac{\partial^2 \rho}{\partial x^2} + k\rho C, \tag{11b}$$

$$\frac{dL}{dt} = \left[u - \frac{D_\rho}{\rho}\frac{\partial \rho}{\partial x}\right]\Big|_{x=L(t)}, \tag{11c}$$

$$u = -\alpha \frac{\partial P}{\partial x}, \tag{11d}$$

$$\rho = \rho_0 + \beta P, \tag{11e}$$

which is to be solved subject to the following boundary and initial conditions:

$$C|_{x=0} = C_0, \quad \frac{\partial C}{\partial x}\Big|_{x=L(t)} = 0, \tag{11f}$$

$$C|_{t=0} = C_I(x) = \begin{cases} C_0 & \text{if } x = 0, \\ 0 & 0 < x \le L_0, \end{cases} \tag{11g}$$

$$\rho|_{t=0} = \rho_I(x), \tag{11h}$$

$$L|_{t=0} = L_0, \tag{11i}$$

$$\frac{\partial P}{\partial x}\Big|_{x=0} = 0, \quad P|_{x=L(t)} = 0. \tag{11j}$$

2.1. Transformation to a fixed domain and nondimensionalisation

In order to compute numerical solutions of model (11), we first transform it from a free boundary problem to one on the fixed spatial domain $\xi \in [0,1]$ (Crank, 1987) using the coordinate change

$$(x,t) \to (\xi, T) = \left(\frac{x}{L(t)}, t\right). \tag{12}$$

We then nondimensionalise the equations. As the spatial variable is mapped to the nondimensional domain $[0,1]$ by the transformation above, we require no rescaling for ξ. The other variables are scaled as follows:

$$\begin{aligned} T &= \hat{T}_{\text{adv}}\tilde{T}, \quad C = C_0\tilde{C}, \quad L = L_0\tilde{L}, \quad X = L_0\tilde{X}, \\ \rho &= \rho_0\tilde{\rho}, \quad u = \frac{L_0}{\hat{T}_{\text{adv}}}\tilde{u}, \quad P = \hat{\pi}\tilde{P}. \end{aligned} \tag{13}$$

Since the cell velocity is created by cell proliferation, the timescale of advection is likewise based on the rate of cell proliferation. That is, $\hat{T}_{\text{adv}} = \frac{1}{C_0 k}$. The system then becomes (on dropping tildes for brevity):

$$\frac{\partial C}{\partial T} + \left[\frac{u}{L} - \frac{\xi}{L}\frac{dL}{dT}\right]\frac{\partial C}{\partial \xi} = \frac{1}{Pe}\frac{1}{L^2}\frac{\partial^2 C}{\partial \xi^2} - \frac{\hat{\lambda}}{Pe}\rho C - \frac{1}{L}\frac{\partial u}{\partial \xi}C, \tag{14a}$$

$$\frac{\partial \rho}{\partial T} + \left[\frac{u}{L} - \frac{\xi}{L}\frac{dL}{dT}\right]\frac{\partial \rho}{\partial \xi} = \frac{D}{Pe}\frac{1}{L^2}\frac{\partial^2 \rho}{\partial \xi^2} + \rho C - \frac{1}{L}\frac{\partial u}{\partial \xi}\rho, \tag{14b}$$

$$\frac{dL}{dT} = \left[u - \frac{D}{Pe}\frac{1}{\rho L}\frac{\partial \rho}{\partial \xi}\right]\Big|_{\xi=1}, \tag{14c}$$

$$u = -\frac{1}{L}\frac{\partial P}{\partial \xi}, \tag{14d}$$

$$\rho = 1 + \hat{\beta}P, \tag{14e}$$

with boundary and initial conditions

$$u|_{\xi=0} = 0, \tag{14f}$$

$$C|_{\xi=0} = C_0, \quad \frac{\partial C}{\partial \xi}\Big|_{\xi=1} = 0, \tag{14g}$$

$$C|_{T=0} = C_I(\xi) = \begin{cases} 1 & \text{if } \xi = 0, \\ 0 & \text{else}, \end{cases} \tag{14h}$$

$$L|_{T=0} = 1, \tag{14i}$$

$$\rho|_{T=0} = \rho_I(\xi) = 1 + \epsilon\cos\left(\frac{\pi}{2}\xi\right), \tag{14j}$$

$$\frac{\partial P}{\partial \xi}\Big|_{\xi=0} = 0, \quad P|_{\xi=1} = 0. \tag{14k}$$

where we have introduced the following dimensionless parameters:

$$\hat{\lambda} = \frac{\lambda \rho_0 L_0^2}{D_C}, \quad D = \frac{D_\rho}{D_C}, \quad \hat{\beta} = \frac{\beta L_0^2}{\alpha C_0 k \rho_0} \quad Pe = \frac{\hat{T}_{\text{diff}}}{\hat{T}_{\text{adv}}} = \frac{C_0 k L_0^2}{D_C}.$$

We note all the dimensionless parameters are non-negative. Here $\hat{\lambda}$ represents the rate of nutrient consumption, D is the ratio between cell and nutrient diffusivity, $\hat{\beta}$ is the compressibility constant, and Pe is the Péclet number.

3. Quantification of growth

3.1. Replicative and quiescent regions

We now introduce the concept of a replicative region where cells can proliferate and a quiescent region where they cannot. We assume that proliferation requires nutrient. Therefore, a replicative region is the part of the tissue where there is sufficient nutrient for proliferation to occur, whilst a quiescent region is the part where there is insufficient nutrient. This translates to tissue growth in the replicative region and no growth in the quiescent region. In the cylindrical yeast colonies experimentally grown by Vulin et al. (2014), nutrient was provided at the base, and it was suggested that the nutrient did not diffuse the whole way through the colony. In that case, we would expect that the quiescent region is near the top of the colony, and the replicative region starts from the base of the colony to where the quiescent region begins (see Fig. 1(a)).

In our model, we will assume that quiescence occurs when the local nutrient concentration, C, is below a certain value, θ. We set $\theta = 10^{-3}$ for all calculations in this paper. We then define the replicative region to be where the concentration, C is above the threshold θ. We use this definition because, in practice, we expect that proliferation will cease when the nutrient level is low, but non-zero.

3.2. Pathlines

We consider tracking points within the growing tissue to be roughly equivalent to tracking the positions of marked cells as the colony grows. Therefore, we employ pathlines of individual cells, $x = X(t)$ (starting from the initial position $X(0) = X_0$) to explore regions of proliferating and quiescent cells within the tissue by tracking cell position. In our full compressible model, the dimensionless equation for the pathlines is given by:

$$\frac{dX}{dT} = \left[u - \frac{D}{Pe}\frac{1}{\rho L}\frac{\partial \rho}{\partial \xi}\right]\Bigg|_{\xi=\Xi}, \tag{15}$$

where $\Xi = X/L(t)$. These pathlines can be used to identify a region of replicative cells that can experience uniform or non-uniform proliferation and a quiescent region where no proliferation occurs.

In addition, we introduce relative pathlines that are defined over the domain $\Xi = X(t)/L(t) \in [0, 1]$, where $X(t)$ represents the pathlines in physical space, and $L(t)$ corresponds to the length of the colony. These space–time diagrams give us a tool to distinguish between uniform and non-uniform proliferation easily. That is, for uniform proliferation over the whole domain, the relative pathlines will be vertical because the relative positions of tagged cells do not change over time. Note this vertical property builds on the assumption that the tissue is incompressible. For instance, if a cell begins halfway up the colony, it will remain at the same relative position as the colony grows longer. If the paths do not satisfy this property, then the proliferation is termed non-uniform. (It is worth noting that if there is no growth in the domain, both the relative pathlines and pathlines in physical space will remain vertical for all times.)

3.3. Examples of simple growth scenarios

To better understand and classify pathlines and the three types of proliferation, we explore four of the scenarios of uniaxial growth from Gallo et al. (2021) that are most relevant to this study. These are presented in Fig. 2. In this section, rather than solving Eq. (14a) for the nutrient, we simply prescribe different nutrient concentration profiles within the colony (Figs. 2(a) to 2(d)). We can then observe the three different types of proliferation: uniform, non-uniform, and no proliferation. The qualitative behaviour resulting from these three types of proliferation are captured in the pathlines of ten initially equally-spaced cells within the colony in Figs. 2(i) to 2(l). Note that, by definition, uniform and non-uniform proliferation can only occur in the replicative region (highlighted in green) with no proliferation in the quiescent region (highlighted in red).

We begin by analysing Case I, where there is a prescribed constant nutrient concentration throughout the colony (see Figs. 2(a)), leading to a constant rate of cell proliferation. This results in the whole domain exhibiting uniform proliferation leading to the relative pathlines being vertical as shown in Fig. 2(e). The corresponding pathlines remain equally spaced since all parts of the colony proliferate at the same rate (see Fig. 2(i)). Examining the length, $L(t)$, we observe the colony is growing at an exponential rate.

By contrast, in Case II the nutrient concentration is linearly decreasing in x (and independent of time) as seen in Fig. 2(b), but still present throughout the entire colony — so all cells proliferate. However, the cells at the base of the colony can proliferate faster than those at the top resulting in non-uniform proliferation. This is shown by the relative pathlines in Fig. 2(f) being non-vertical. As a consequence, the pathlines (Fig. 2(j)) of initially equidistant points are not equidistant at times $t > 0$. The corresponding length still grows at an exponential rate but slower than in the case of uniform concentration (Case I).

Now turning to Gallo et al. (2021)'s Case III, where we have a replicative region of constant length $H < L(0)$ (which is less than the length of the colony) with constant concentration within that region as shown in Fig. 2(c). The pathlines shown in Fig. 2(k) reveal a green replicative region proliferating uniformly and a red quiescent region with no proliferation. This leads to non-uniform proliferation over the whole domain because only a part of the domain is capable of proliferation. The non-uniform proliferation is evident from the fact that the relative pathlines are non-vertical in Fig. 2(g). Furthermore, as both the nutrient concentration and the size of the replicative region are fixed, we observe the colony grows at a linear rate (see Fig. 2(k) at $x = L_0$).

Finally, we analyse Case IV where we also have a fixed replicative region, but with a linearly decreasing nutrient concentration as shown in Fig. 2(d). Similar to Case III, we observe the relative pathlines are non-vertical meaning the whole domain experiences non-uniform proliferation and the global grow remains linear (see Figs. 2(h) and 2(l) respectively). However, the key distinction compared to Case III is the replicative region experiences non-uniform proliferation instead of uniform. A summary of the comparison between the four cases is provided in Table 1.

In our PDE model, the classification of uniform and non-uniform proliferation in the replicative region and no proliferation in the quiescent region is the same as described above. That is, for uniform proliferation, we require constant access to nutrient throughout the colony. However, in our model, the nutrient consumption rate is given by $\hat{\lambda}\rho C/Pe$ in Eq. (14a) meaning that the nutrient will always be non-constant, similar to Cases II and IV. Hence, we conclude that our model can only experience non-uniform proliferation in the replicative region and no proliferation in the quiescent region with the overall proliferation across the domain being non-uniform. In physical space, this leads to curved paths in the (green) replicative region and straight lines in the (red) quiescent region.

We can derive the pathlines using our continuum model in all four cases by assuming that the tissue is incompressible (i.e., taking the limit $\hat{\beta} \to 0$ in Eq. (14e)) and prescribing the nutrient concentration $C(\xi, T)$ instead of solving Eq. (14a) (for instance, in Case I, we set $C(\xi, T) = 1$ for all space and time). We can then solve Eq. (19) for u which allows us to then solve for the pathlines.

4. Incompressible system

We will first consider the model in the case where the cells are incompressible, which corresponds to the limit $\hat{\beta} \to 0$. Eq. (14e), then tells us that the cell density is constant, so $\rho = 1$. This coincides with

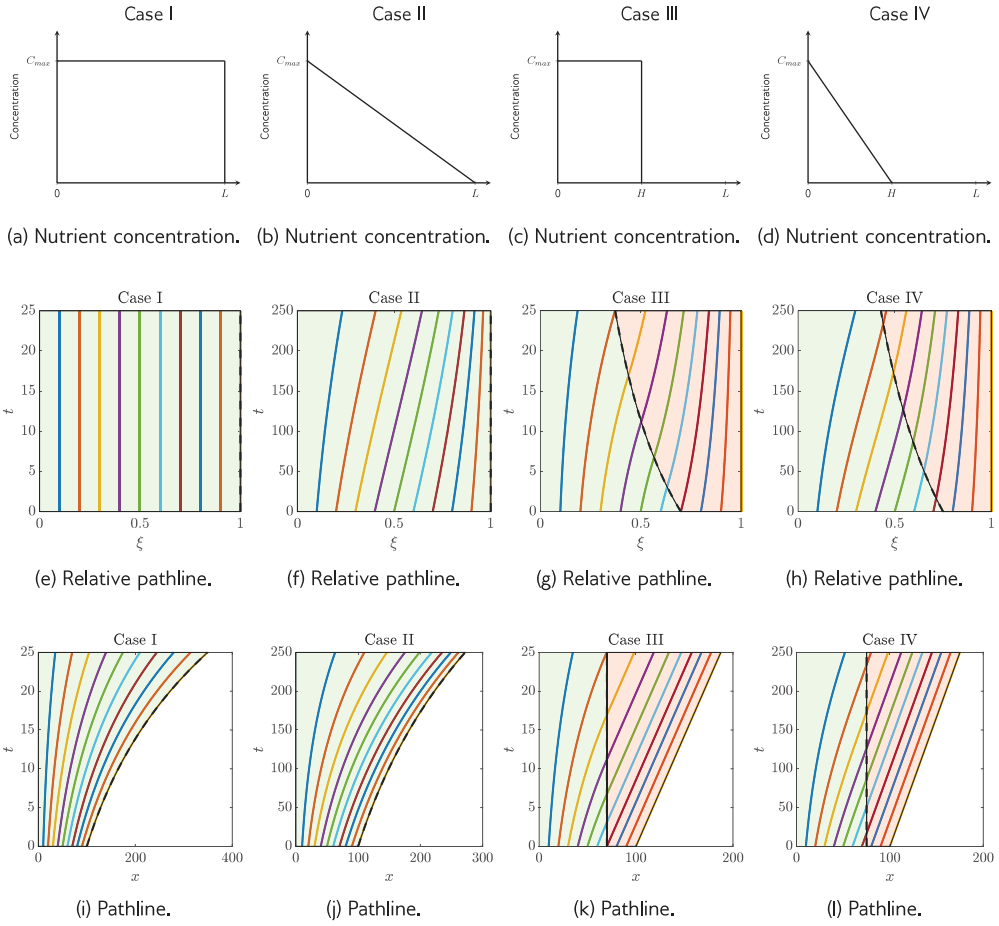

Fig. 2. Four different types of modelling scenario for uniaxial growth from Gallo et al. (2021). **Top row:** Nutrient concentration prescribed within the domain independent of time. The nutrient can either be present throughout the domain $0 \leq x \leq L(t)$ or only in part of it $0 \leq x \leq H$ (where H is a constant); C_{max} denotes the maximum nutrient concentration. **Middle row:** Relative pathlines ($\Xi = X(t)/L(t)$) provides a tool to distinguish between uniform and non-uniform proliferation in the replicative region. Green regions represent the replicative part of the colony while red depicts quiescent. **Bottom row:** Corresponding pathlines, $X(t)$ showing the local and global growth behaviour of the colony with the length $L(t)$ starting at $x = L_0$. (**a, e, i**) Case I has only a replicative region and a constant nutrient concentration. (**b**, **f**, **j**) Case II only has a replicative region but with a linearly decreasing nutrient concentration. (**c**, **g**, **k**) Case III has a fixed replicative region with a constant nutrient concentration. (**d**, **h**, **l**) Case IV has a fixed replicative region with a linearly decreasing nutrient concentration.

Table 1
Summary of the possible types of domain proliferation and growth. We assume here the nutrient concentration is continuous in the parts of the domain where nutrient is available. Furthermore, we assume the nutrient availability of each case is fixed for all time.

	Nutrient availability	Proliferation in replicative region	Global proliferation	Growth globally	Relative pathlines behaviour
Case I	Whole domain: constant	Uniform	Uniform	Exponential	Vertical
Case II	Whole domain: non-constant	Non-uniform	Non-uniform	Exponential	Non-vertical
Case III	Part of domain: constant	Uniform	Non-uniform	Linear	Non-vertical
Case IV	Part of domain: non-constant	Non-uniform	Non-uniform	Linear	Non-vertical
	No nutrient available (Degenerate case)	NA	No proliferation	No growth	Vertical

the constitutive assumption made by Neville et al. (2006). Eq. (14b) then becomes:

$$\frac{\partial u}{\partial \xi} = LC. \tag{16}$$

whilst (14c) simplifies to:

$$\frac{dL}{dT} = u|_{\xi=1}\,. \tag{17}$$

This implies that the top of the colony travels with the advective cell velocity, and the advective cell velocity is equal to the local cell velocity. We also note that Eq. (15) for the pathlines $X(t)$ simplifies to

$$\frac{dX}{dT} = u|_{\xi=\Xi(t)}\,, \tag{18}$$

where $\Xi = X/L(t)$. Using the boundary condition (14f), we can rewrite Eq. (16) as:

$$u(\xi, T) = \int_0^{\xi} L(T)C(\xi^\star, T)\, d\xi^\star. \tag{19}$$

We now have only four unknown dependent variables. This is because the cell density is known to be constant. We note that it is redundant to calculate the pressure in the incompressible model since it appears in only one equation and is not used to calculate the other three dependent variables. We thus drop Eq. (14d) from the model. In addition, we substitute Eq. (16) into Eq. (14a) simplifying the last term in Eq. (14a) to C^2. The incompressible model is therefore:

$$\frac{\partial C}{\partial T} + \left[\frac{u}{L} - \frac{\xi}{L}\frac{dL}{dT}\right]\frac{\partial C}{\partial \xi} = \frac{1}{Pe}\frac{1}{L^2}\frac{\partial^2 C}{\partial \xi^2} - \frac{\hat{\lambda}}{Pe}C - C^2, \tag{20a}$$

$$u = L\int_0^{\xi} C(\xi^\star, T)\, d\xi^\star, \tag{20b}$$

$$\frac{dL}{dT} = u|_{\xi=1}\,, \tag{20c}$$

with boundary and initial conditions

$$u|_{\xi=0} = 0, \tag{20d}$$

$$C|_{\xi=0} = 1, \quad \left.\frac{\partial C}{\partial \xi}\right|_{\xi=1} = 0, \tag{20e}$$

$$C|_{T=0} = C_I(\xi) = \begin{cases} 1 & \text{if } \xi = 0, \\ 0 & \text{else,} \end{cases} \tag{20f}$$

$$L|_{T=0} = 1. \tag{20g}$$

Notice now that the incompressible model contains only two parameters, Pe and $\hat{\lambda}$. Furthermore, note that the $\frac{1}{L}\frac{\partial u}{\partial \xi}C = C^2 \geq 0$ term in Eq. (20a) always acts as a sink in the incompressible system. (However, as we will see Section 5.2, in the compressible system the $\frac{1}{L}\frac{\partial u}{\partial \xi}C$ term can change sign, and thus act as a local source or sink.)

4.1. Numerical simulations

We use the method of lines (Sadiku and Obiozor, 2000; Driscoll and Braun, 2017) to solve the above system of PDEs. This technique is a finite difference method that can solve a large class of PDEs numerically by discretising space while leaving time continuous. This allows us to convert our PDE into a system of ordinary differential equations and solve them using well-established numerical methods. Illustrative results can be seen in Fig. 3.

We start by setting $Pe = 0.01$, so nutrient transport is mainly by diffusion, and assume a moderate rate of nutrient consumption, $\hat{\lambda} = 1$. Then, in Fig. 3(a) we see the nutrient decreases over time and with distance up the colony, as nutrient is depleted by cell proliferation. A significant feature of this incompressible model is that the minimum nutrient concentration always occurs at the top of the colony ($C(\xi = 1, T)$) for all parameter values. However, we will see this is not always the case in the compressible model.

As foreshadowed in Section 3.2, the replicative region experiences non-uniform proliferation. (Note that the relative pathline starting from

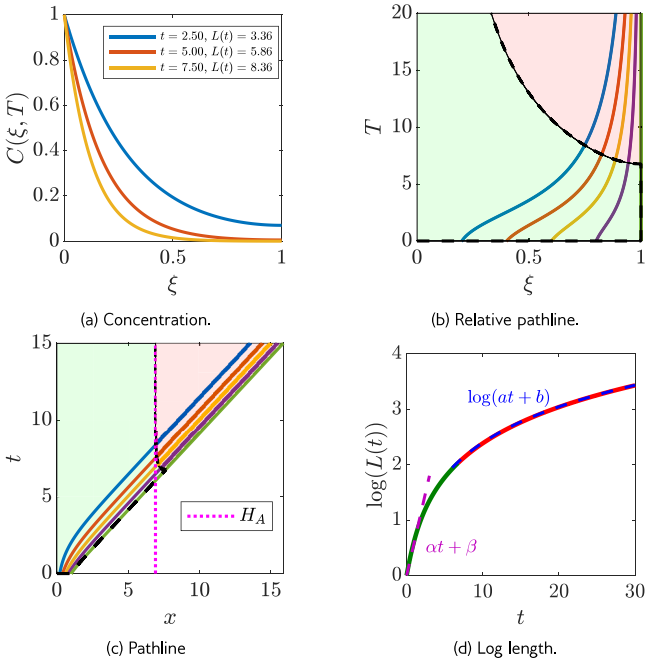

Fig. 3. Numerical solutions of the incompressible case with Péclet number $Pe = 0.01$ and nutrient consumption rate $\hat{\lambda} = 1$. **(a)** Time-lapse image of monotonically decreasing nutrient concentration. **(b)** Relative pathlines displaying non-uniform proliferation in the replicative region (green) and no proliferation in the quiescent region (red). **(c)** Pathlines showing non-linear growth in the green replicative region and no growth in the red quiescent region resulting in overall length growing linearly. $H_A = 6.91$ is given in purple dotted line derived in Section 4.2. **(d)** Log length showing non-linear property (green curve) with exponential growth for early times and linear property (red curve) as we transition from replicative to quiescent region. The dashed line and curve are artificially prescribed linear function (purple) and logarithmic function (blue) respectively. The parameters used are $\alpha = 0.6$, $\beta = 0$, $a = 1$, and $b = 1$.

$t = 0$ at $\xi = 1$ is always vertical since our kinematic boundary condition states that a cell starting at the top of the colony always remains there.) We see that the relative pathlines differ from the base cases in Fig. 2 due to the fact that the length of the replicative region does not corresponds to either of the illustrative situations. Instead, colony growth is coupled with the nutrient concentration in Fig. 3(a) which dictates regions of proliferation by the threshold θ described in Section 3.1. At early times the entire colony is capable of proliferation, however, once the colony becomes sufficiently large, the replicative region becomes constant in length. The results in Fig. 2 thus lead us to expect that the colony length will grow exponentially at early times, and linearly at later times. We hence examine the logarithm of the colony length, as shown in Fig. 3(d) which we expect to be linear for exponential behaviour and logarithmic for linear behaviour. Comparison with prescribed linear and logarithmic functions, shown by the purple dashed line and blue dashed curve, respectively, confirms our prediction. As expected, the log length plot indicates exponential growth for early times ($t \lesssim 5$) when the replicative region (green curve) comprises the entire colony, non-linearity in the transition phase, and linear growth once a quiescent region (red curve) becomes clearly established ($t \gtrsim 10$).

We now consider the effects of varying the two nondimensional parameters $\hat{\lambda}$ and Pe, the results of which are summarised in Fig. 4. Firstly, we begin by analysing the impact of the rate nutrient consumption by cells. Since $\hat{\lambda}$ represent the dimensionless rate of nutrient consumption, if $\hat{\lambda} \ll 1$, the nutrient required for cells to proliferate is small. We would then expect the nutrient concentration at the top of the colony to be relatively high and the corresponding colony length to be long (due to the high rate of proliferation). These behaviours are exactly what we observe in the top row of Fig. 4. I.e. In Fig. 4(a) as $\hat{\lambda} \to 0$ we identify a large nutrient concentration at the top of the colony and

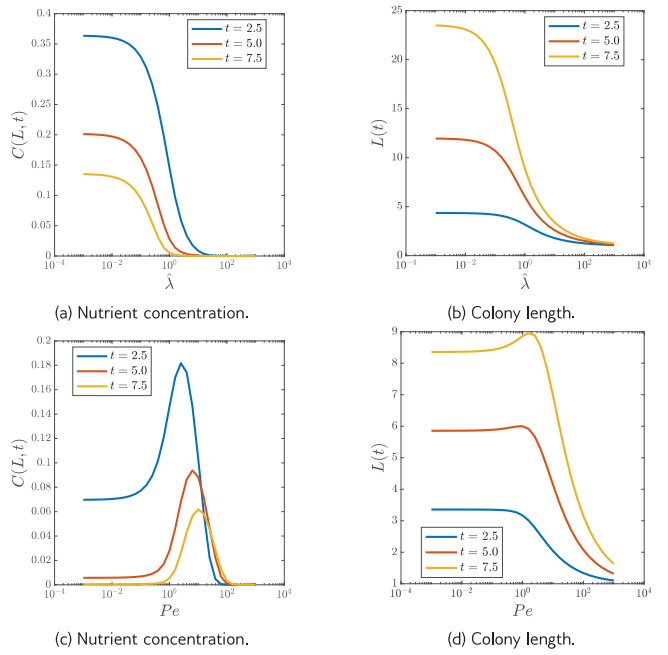

Fig. 4. Incompressible solutions at three time intervals plotted against varying one parameter (Pe or $\hat{\lambda}$) whilst holding the other constant at one. **(a)** Time-lapse image of nutrient level calculated at the top of the colony $C(L,T)$ showing a monotonically decreasing trend over time. As the nutrient consumption rate $\hat{\lambda}$ increases from small to large, the concentration is also reduced. **(b)** Colony length at three different periods displaying an increase in length chronologically. The length monotonically decreases as $\hat{\lambda}$ becomes large, mirroring the qualitative behaviour of the nutrient concentration in **(a)**. **(c)** Varying Péclet reveals the nutrient concentration is controlled by a balance of advection and diffusion with nutrient consumption. An equal balance between the two creates an optimal amount of nutrient spread throughout the colony. **(d)** Corresponding length mirroring the qualitatively shape to the nutrient concentration in **(c)**. However, the length increases over time.

as $\hat{\lambda}$ increases the concentration monotonically decreases. Furthermore, we see a clear relationship between the nutrient concentration C, and colony length (Fig. 4(b)) as the proliferation is given by $k\rho C$. Hence, when the cells in the colony have plenty of access to nutrient ($\hat{\lambda} \ll 1$) we indeed observe the length of the colony is longer. This relationship is a realistic reflection of the physical behaviour we expect from biological systems such as cylindrical yeast colonies. We also note that when $\hat{\lambda} \ll 1$ the colony will experience exponential growth across the whole domain because the whole colony have access to nutrient as shown in Fig. 4(b). This is analogous to Cases I and II in Fig. 2.

Secondly, we consider the effect of varying the Péclet number (Pe) which is defined as the ratio between the time scale of diffusion over the time scale of advection. For a small Péclet number, the distribution of the nutrient is governed by diffusion and consumption. This can be explained by taking the limit as $Pe \to 0$ in Eq. (20a) which would result in advection and time derivative terms to be negligible. On the other hand, if $Pe \gg 1$ we would expect the system to be heavily influenced by advection. Hence, the evolving concentration and colony length are dependent on a balance between diffusion with nutrient consumption and advection.

The variation in the Péclet numbers (Pe) is captured in Figs. 4(c) and 4(d) and verifies our predictions in the previous paragraph. We observe the nutrient and length throughout the domain remain constant for $Pe \ll 1$ due to nutrient and cells diffusing rapidly throughout the domain. In addition, there is a clear relationship between nutrient concentration and colony growth. That is, as the Péclet number increases we notice an optimal concentration and length are met as diffusion and advection are both equally acting over the domain. However, once advection takes over for $Pe \gg 1$ we see both the concentration and length decrease because the nutrient is only getting transported through cell velocity.

4.2. Analytical approximation for the length of the replicative region for $Pe \ll 1$

In our simulations in Fig. 4, we observe that, once the colony becomes quite large, the size of the replicative region can remain fixed despite domain growth, similar to Fig. 3(c). This explains the observed linear growth of the colony. We now explore what determines the size of the replicative region as $L \to \infty$ in the case where the Péclet number is small (nutrient transport by advection is negligible) which we believe is likely to pertain to biological growth. If we take the limit $Pe \to 0$, and write the governing equation for nutrient concentration (20a) in terms of the Eulerian spatial variable x, we find that

$$\frac{\partial^2 C}{\partial x^2} = \hat{\lambda} C \tag{21}$$

where $C = 1$ at $x = 0$, $C_x = 0$ at $x = L(t)$. Solving (21) subject to these mixed boundary conditions yields

$$C(x,t) = \frac{1}{\cosh\left(\sqrt{\hat{\lambda}} L\right)} \cosh\left[\sqrt{\hat{\lambda}}(L - x)\right] \tag{22}$$

We observe that Eq. (22) is a monotonically decreasing function on the domain $0 \le x \le L(t)$. Recall that we have imposed that cells are replicative when $C > \theta$ and quiescent when $C < \theta$. Hence, we set the value of H to be the spatial position where the nutrient concentration C is equal to the tolerance θ. Setting $C(H,t) = \theta$ in Eq. (22) and rearranging gives:

$$H = L - \frac{1}{\sqrt{\hat{\lambda}}} \cosh^{-1}\left(\theta \cosh \sqrt{\hat{\lambda}} L\right). \tag{23}$$

There is no explicit time dependence in Eq. (23). However, as we are solving on a growing domain, the length is a monotonically increasing function and thus $L \to \infty$ as $t \to \infty$. Hence, we take the limit $L \to \infty$ to approximate the behaviour of H as t gets large. We define this quantity to be H_A, which provides an analytic approximation for H when the colony is large. It is given by:

$$H_A = \lim_{L\to\infty} H = -\frac{1}{\hat{\lambda}} \ln \theta, \tag{24}$$

As we have set $\theta = 10^{-3}$, we can re-write (24) as

$$H_A(\hat{\lambda}) = \lim_{L\to\infty} H = \frac{3}{\sqrt{\hat{\lambda}}} \ln 10. \tag{25}$$

Evaluating Eq. (25) for $\hat{\lambda} = 1$, we find that $H_A \approx 6.91$. Comparing this approximation (purple dashed line) in Fig. 3(c) with $Pe = 0.01$ and $\hat{\lambda} = 1$, we observe that the numerical solution tends to 6.92, in close agreement with our analytical approximation.

5. Compressible system

The full compressible model Eq. (14) as derived in Section 2 has four non-dimensional parameters, $\hat{\beta}, D, Pe$, and $\hat{\lambda}$. Compared to the incompressible model, there are two additional parameters the compressibility and diffusion coefficient, $\hat{\beta}$ and D. As previously discussed, the limit $\hat{\beta} \to 0$ implies that the system is incompressible ($\rho = 1$), otherwise the system is compressible with variable density, $\rho = \rho(\xi, T)$. The coefficient, D, is defined as the ratio of the cell diffusion to nutrient diffusion. The smaller D is, the slower cells diffuse relative to the nutrient.

5.1. Numerical simulations

We now solve the full compressible model, using the method of lines. We begin by setting all parameter values to one and present

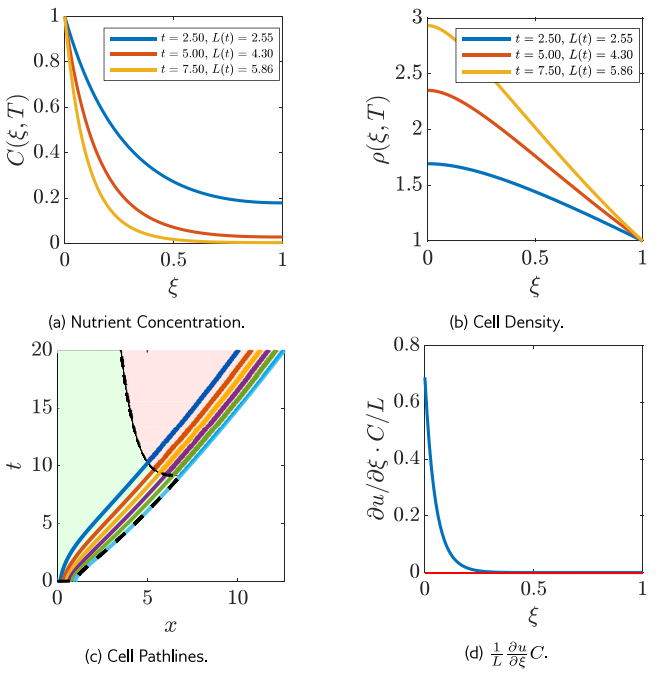

Fig. 5. Compressible solution with $Pe = \hat{\beta} = \hat{\lambda} = D = 1$. **(a)** Monotonically decreasing nutrient concentration. **(b)** Non-constant density over the entire domain. The initial condition used for cells density is $\rho_I(\xi) = 1 + \epsilon\cos(\frac{\pi}{2}\xi)$ where $\epsilon = 0.01$. **(c)** Pathlines depicting a replicative region (green) and a quiescent region (red). **(d)** Non-negative product between advective velocity gradient and nutrient concentration taken at $T = 7.5$.

the results in Fig. 5. When compared to the incompressible results, we see the nutrient concentration (Figs. 3(a) and 5(a)) and pathlines (Figs. 3(c) and 5(c)) are qualitatively similar. In this case, we observe the advective term acts as a local sink and thus we have qualitative similar results as the incompressible case (Fig. 5(d)). However, in contrast to the incompressible case, the cell density can now vary with distance up the colony as shown in Fig. 5(b). As expected, for the same value of Pe and $\hat{\lambda}$, we found the length of the colony is shorter than in the incompressible case (incompressible result not shown). Note, as we have established that the whole domain can either experience non-uniform or no proliferation in Section 3.2. Hence, we will only presented the pathlines as the relative pathlines will remain similar to Fig. 3(b) for the compressible model.

We now consider the effect of varying each of the parameters in turn, whilst holding the others fixed at one. We quantify their effect by plotting cell density at the base of the colony, $\rho(\xi = 0, T)$ (blue) and colony length $L(T)$ (red) at a fixed time T, with the results summarised in Fig. 6. Note that $\rho(\xi = 0, T)$ is the maximum cell density in the colony.

First, we discuss the variation in the compressibility, $\hat{\beta}$, as shown in Fig. 6(a). We note that when $\hat{\beta} \ll 1$, the results are qualitatively similar to that found in the incompressible case. We observe that as $\hat{\beta}$ increases, the maximum density, $\rho(\xi = 0, T)$, increases and the length, $L(T)$, decreases, which makes sense because a denser colony will have a shorter length due to compressed cells requiring less space.

Next, we shift our focus to the impact of varying the diffusion coefficient D, as depicted in Fig. 6(b). Recall that D is defined as the ratio of cell diffusion coefficient to nutrient diffusion coefficient. Therefore, for $D \ll 1$, nutrient diffuses rapidly throughout the colony, leading to a near constant nutrient concentration and causing negligible change to the cell density and colony length. On the other hand, when D exceeds one, cell diffusion overtakes nutrient diffusion, making cells more motile. When D is less than one, the changes in cell density and colony length is barely visible, as the system is dominated by nutrient diffusion and cells move mainly by advection. As D increases and the random motion of the cells increases, we observe a decrease in cell density and an increase in colony length since cells experience less compression.

The impact of varying the Péclet number (Pe), which represents the ratio of the diffusion time scale to the advection time scale, on the observed colony length and cell density is illustrated in Fig. 6(c). Our findings show that, as Pe increases, the colony length undergoes a decrease, except for a minor increase when Pe is around one. Moreover, we observe that the cell density initially increases and then decreases, peaking when Pe reaches approximately ten. These results can be attributed to the balance between diffusion and advection processes, similar to that analysed in the incompressible case. Specifically, when Pe is much smaller than one, the diffusion process dominates, leading to the rapid dispersion of nutrient and cells throughout the colony. This results in a longer colony length but a lower cell density. As Pe gradually increases to around ten, the balance between diffusion and advection is attained, allowing cells to actively move and be transported along with the cell velocity, which leads to an optimal cell density. As advection becomes the dominant process, the nutrient and cells are mainly carried along with the cell velocity, causing the colony length to decrease. Finally, at higher Pe values, advection dominates over diffusion, resulting in a decrease in both the cell density and colony length, as cells and nutrient are primarily transported up the colony by the cell velocity.

The effect of varying the nutrient consumption coefficient $\hat{\lambda}$ is investigated in Fig. 6(d). For $\hat{\lambda} \ll 1$, we observe both the cell density and colony length to be relatively large. This can be attributed to the fact that cells require minimal nutrient to proliferate, leading to an increased number of cells being produced and ultimately resulting in a larger colony length and cell density. As $\hat{\lambda}$ increases, we observe a rapid decrease in both the cell density and colony length. This is because cells require a greater amount of nutrient to proliferate, resulting in a lower number of cells in the colony.

5.2. Non-monotonically decreasing nutrient concentration

Recall that in the incompressible case and for moderately large values of the parameters in the compressible case, the nutrient concentration is found to decrease monotonically, as shown in Figs. 3(a) and 5(a). This is because the advection term in Eq. (14a), $\frac{1}{L}\frac{\partial u}{\partial \xi}C \geq 0$, is a sink. Furthermore, in the incompressible case, using Eq. (16), it is straightforward to show that $\frac{1}{L}\frac{\partial u}{\partial \xi}C = C^2 \geq 0$.

However, under the presence of high compression ($\hat{\beta} \geq 1$) and negligible nutrient consumption ($\hat{\lambda} \ll 1$), we found that the nutrient concentration exhibits unexpected behaviour by not monotonically decreasing, as observed in Fig. 7(a). This is because the advection term, $\frac{1}{L}\frac{\partial u}{\partial \xi}C$, can be negative, thus acting as a local source as seen in Fig. 7(d). This is in contrast to the results in Figs. 3(a) and 5(a) where we observe that the nutrient concentration approaches zero at the end of the domain.

Furthermore, the pathlines also exhibit unusual behaviour. Owing to the non-monotonic nutrient concentration, the domain may exhibit two replicative regions separated by a quiescent region in the middle, as shown in Fig. 7(c). This is because the nutrient concentration near the middle of the colony can drop below the threshold θ, while the concentration at the top and bottom of the colony remains above it (see black dash curve Fig. 7(c), $t \approx 15$). This is different from the pathlines shown in Figs. 3(c) and 5(c) where there is only one replicative region and one quiescent region. Interestingly, however, we observe that the plots of density are qualitatively similar in Figs. 5(b) and 7(b).

In addition, from the long-term behaviour we observe the second proliferative region (the one nearest $x = L$) eventually disappear as the colony gets very long. This can be explained from a physical perspective. That is, the nutrient in the second proliferative region will be consumed and not replenished. This is because the only source of

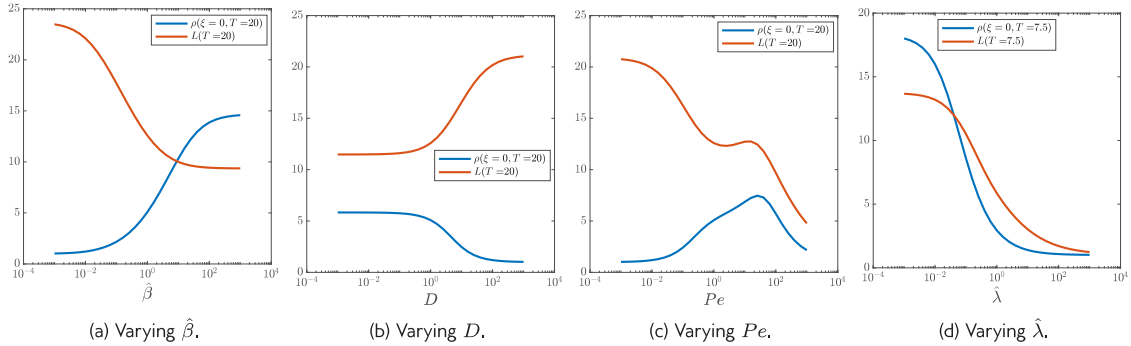

(a) Varying $\hat{\beta}$. (b) Varying D. (c) Varying Pe. (d) Varying $\hat{\lambda}$.

Fig. 6. Compressible solution of density $\rho(\xi,T)$ at the base of the colony ($\xi=0$) and colony length, $L(T)$ for fixed time T. One parameter is varied at a time whilst holding all other parameters constant at one. **(a)** Varying the compressibility coefficient $\hat{\beta}$. **(b)** Varying the diffusion coefficient (D) which is the ratio of cell diffusivity to nutrient diffusivity. **(c)** Varying the Péclet number Pe which is the ratio of time scale of diffusion over time scale of advection. **(d)** Varying the nutrient consumption rate $\hat{\lambda}$.

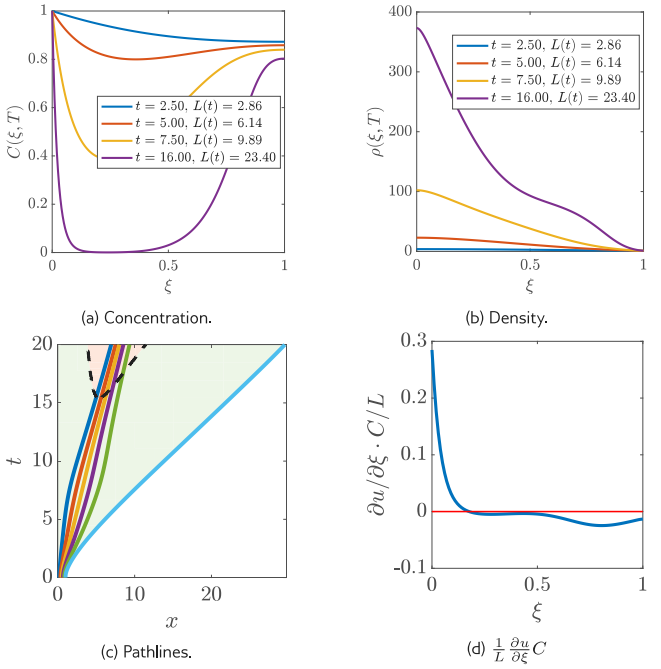

(a) Concentration. (b) Density. (c) Pathlines. (d) $\frac{1}{L}\frac{\partial u}{\partial \xi}C$

Fig. 7. Counter-intuitive case where the nutrient concentration exhibits a positive gradient for $\hat{\lambda} \ll 1$. Here the parameters used are $\hat{\lambda}=0.01, Pe=1, \hat{\beta}=100, D=1$. **(a)** Time-lapse images of nutrient concentration displaying an increase in the concentration within the domain. **(b)** Cell density plot showing the density increasing at an exponential rate. **(c)** Pathlines containing two replicative regions (green) and a quiescent region (red). **(d)** Advective cell velocity changes sign within the domain causing the change in concentration gradient and creation of two replicative regions taken at $T=7.5$.

nutrient is on the left hand side of the colony. Therefore, nutrient in the second proliferative region can only be replenished from the left-hand side, and this requires the nutrient to travel across the quiescent region without any cell proliferation which is physically impossible. We would also like to note that this type of behaviour is unlikely to occur in yeast growth, where we expect $\hat{\lambda} \gg 1$ (Vulin et al., 2014; Tam et al., 2019) (also see Section 6). Nonetheless, this scenario may occur in other types of physical systems that experience uniaxial growth.

6. Application to cylindrical yeast colonies

We now apply our model to the cylindrical yeast colony growth scenario from Vulin et al. (2014). Given the lack of data on the compressibility of these colonies, we begin by using the incompressible model which requires the values of only two dimensionless parameters, $\hat{\lambda}$ and Pe, where:

$$Pe=\frac{C_0 k L_0^2}{D_C}, \qquad \hat{\lambda}=\frac{\lambda \rho_0 L_0^2}{D_C}. \tag{26}$$

From Vulin et al. (2014) it was reported the diffusion of nutrient, $D_C=5.184\times10^{-7}$ m^{2}h^{-1}, the growth rate of single cells $kC_0=0.59$ h^{-1} and using interpolation we found the initial colony height as $L_0=2\times10^{-4}$ m. Therefore, we calculate that $Pe\approx0.05$. Likewise, Vulin et al. (2014) also reported the nutrient consumption rate $q(\rho_0,C_0)=\lambda\rho_0C_0=19728$ mol h^{-1}m^{-3} and initial concentration $C_0=55$mM. Hence, using the reported values we get $\hat{\lambda}\approx30$.

We simulate the model using these values and plot the pathlines (using dimensional variables) in Fig. 8. We observe that the colony experiences exponential growth for early times ($t\sim<3$), later transitioning to linear growth (as observed in experiments). Furthermore, at dimensional time $t=350$ hours, Vulin et al. (2014) reported that in the experiments the colony has dimensional length approximately 6.5 mm; by comparison, our model predicts a value of $L\approx7.8$ mm (see Fig. 8). Thus, our model shows reasonable agreement with the data. This is further supported by comparing the experimental result (purple dashed line) to the simulation over the whole growth period.

Although it was not measured experimentally, our model can be used to predict the length of the replicative region. From our simulation, the numerical solution tends to $H\approx0.25$ mm (indicated by the dashed line in Fig. 8). Since, in this case $Pe\ll1$, we can also use the analytical approximation obtained in Section 4.2; from Eq. (25) we get the dimensionless value $H_A\approx1.26$ which corresponds to a dimensional length of approximately 0.25 mm, in agreement with the simulation. This suggests that the simple approximation formula (25) may be of practical use in estimating the size of the proliferative region in yeast. Our prediction indicates that, at later times, the replicative region appears to form only a small proportion of the colony; this echoes the observation in multicellular tumour spheroid growth that, once the spheroid has become reasonably large, cell proliferation is confined to a thin outer rim close to where nutrient is supplied (Byrne and Chaplain, 1997).

Whilst the agreement between the model and experiment is pleasing given that model contains only two parameters, and the values of both were taken from published data rather than fitted, we note that the model does appear to overestimate the colony length slightly. Based on the results in Section 5, this suggests that the colony may, in fact, be compressible to some extent. We hence simulate the compressible model with $Pe=0.05$, $\hat{\lambda}=30$ as before, and fixing $D=0.1$ since, although we do not have experimental data for this parameter, we consider that the random motility coefficient for the cells is likely to be much lower than that for the nutrient. We find that taking $\hat{\beta}=0.2$ gives a predicted length for the colony at of 6.7 mm (see Fig. 9(a)) — better agreement than for the incompressible model. The predicted length of the proliferative region is also smaller, at 0.19 mm. The corresponding

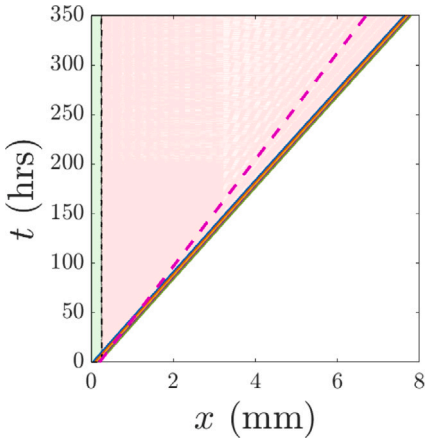

Fig. 8. Dimensional incompressible pathlines to predict cylindrical yeast behaviour ($Pe = 0.05$ and $\hat{\lambda} = 30$) using estimated parameters values formulated from experimental data. The length of the green replicative region is approximately 0.25 mm. The purple dashed line is from the experimental measurements of Vulin et al. (2014).

prediction of the cell density profile after 350 h is shown in Fig. 9(b) (where we have taken the value $\rho_0 = 1.1$ g/mL from Vulin et al. (2014)), and indicates a significant, and almost linear, decrease in density with distance up the colony. Whilst we are not aware of any published measurements of cell density variations in colonies, this is a prediction of our model that could be verified in future experiments. Moreover, comparing the growth of the whole colony over time, we observe that the compressible simulations agrees more closely with the experimental data (purple dashed line) as shown in Fig. 9(a).

7. Discussion

In this paper, we have developed and investigated a system of reaction–advection–diffusion equations to model nutrient-limited uniaxial growth of a tissue. A novel feature of our model, compared to previous works such as Neville et al. (2006), Gallo et al. (2021), is that we have relaxed the assumption that the tissue is incompressible. We began our analysis by classifying the different types of proliferation and growth modes possible and deduced that our model can only undergo non-uniform proliferation. We defined replicative and quiescent regions within the tissue, where the nutrient levels are sufficient or insufficient, respectively, for cell proliferation to occur. By introducing pathlines, we were able to track the movement of cells as the tissue grows, providing further information about cell proliferation.

On making the simplifying assumption that the tissue is incompressible (so the cell density is constant, $\rho = 1$) we observed that the nutrient concentration monotonically decreases over time and space due to the nutrient consumption by the cells. Initially, when the tissue is small, cells have sufficient nutrient to proliferate throughout, and so the tissue length grows exponentially in time. However, as the tissue gets longer there eventually comes a point at which nutrient can only penetrate a certain depth into the tissue before it is used up. Thus, at later times, the length of the proliferative region tends to a constant, and the length of the tissue grows linearly. This is consistent with the experimental observation made by Vulin et al. (2014) and the results from Gallo et al. (2021). For the incompressible system, in the limit of small Péclet number, we derived an analytical approximation for this eventual length of the replicative region, H given in Eq. (25).

Turning to the full compressible model, we found the nutrient concentration and pathlines were qualitatively similar to the incompressible case for a wide range of the model parameters. However, the cell density can vary quite considerably within the tissue in the compressible model. In practice, this means knowing the nutrient concentration and pathlines from experiments would not be sufficient to unambiguously identify all the parameters in the model. Instead, we would require experimental data on cell density.

Interestingly, for a compressible system ($\hat{\beta} \geq 1$) with negligible nutrient consumption rate ($\hat{\lambda} \ll 1$), we observed some counter-intuitive behaviour. Specifically, the nutrient concentration curve can become non-monotonic over the domain, resulting in the colony having two replicative regions and a quiescent region. We found this behaviour could be attributed to the advection term acting like a local nutrient generating source instead of a typical sink under these conditions. Whilst we are not aware of such behaviour having been observed in a biological system to date, it is an interesting prediction of our model that might be verified by future experiments.

One application of the model is the experimental system described by Vulin et al. (2014), who showed that controlling the nutrient supply at the base of yeast colonies can restrict the growth of the colonies in an uniaxial direction with no lateral expansion (see Fig. 1). For reasonably large colonies, they observed that the growth rate of the colony length was linear in time. This was hypothesised to result from a non-uniform distribution of nutrients within the colony, resulting in a fixed-length replicative region. Mathematical modelling by Gallo et al. (2021) showed that a fixed-length replicative region does indeed result in linear growth, consistent with what was observed in experiments, and showed how pathlines might be used to infer the nutrient distribution within the colony.

However, the work of Gallo et al. (2021) used a simple cellular automata model coupled with a prescribed nutrient concentration, with the concentration profile assumed to be constant in time. This assumption was a major limitation of their model, as in general, we expect nutrient levels to vary in time as the colony expands. We overcame this limitation in our work by coupling nutrient concentration with domain growth so the nutrient concentration could vary in time and space. In addition, their implementation and derivation of the cellular automata model and continuum paths respectively assumed the cells were incompressible. This can be directly linked to our continuum incompressible model in Section 4 as we can derive the same pathlines as Gallo et al. (2021) by prescribing the nutrient concentration in the same way. But in addition to recapitulating the linear growth observed for large colonies, our incompressible model reveals an initial exponential phase of growth when the colony is small, and also allows us to predict the length of the proliferating region.

Using parameter values from Vulin et al. (2014), the incompressible model was able to make a prediction of the length of the colony after 350 h which was in reasonable agreement with the experimental measurements. However, by using the compressible model with the experimentally-determined values of the Péclet number and nutrient consumption rate, $\hat{\lambda}$, and fixing $D = 0.1$, we were able to obtain better agreement between model and experiment by setting $\hat{\beta} = 1$. This is consistent with the possibility that yeast colonies are, to some degree, compressible (although, of course, other explanations are possible). As our models generate predictions of the length of the replicative region and, in the compressible case, the variations in cell density with distance up the colony, future experimental measurements of these quantities would allow our model to be validated (or falsified).

Like all models, we have made simplifying assumptions regarding cell behaviour. Two mechanisms that we have neglected here might also account for the over-estimation of the colony length by the incompressible model: contact-inhibition of cell proliferation, and death and necrosis of the cells in the quiescent zone. Contact inhibition would tend to reduce the proliferation rate of cells when the pressure (or local cell density) is high, and this could be incorporated in our model by making the cell proliferation function decrease at high pressures (or cell densities). Death and degradation of cells in the quiescent region would cause a reduction in the biomass of the colony, and correspondingly, a reduction in colony length. This could be incorporated into our model by introducing an additional variable for the density of dead cells, and introducing terms for cell death and decay of cell material into

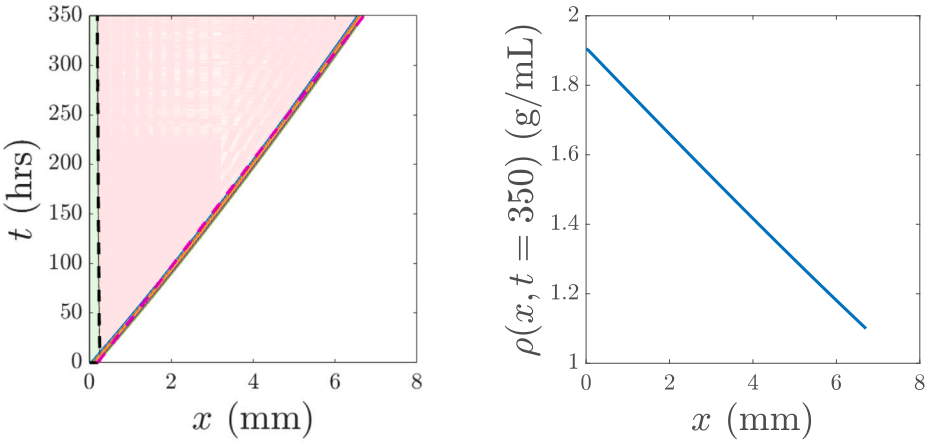

(a) Dimensional pathlines. (b) Dimensional density.

Fig. 9. Applying the compressible model to predict cylindrical yeast behaviour ($Pe = 0.05$, $\hat{\lambda} = 30$, $D = 0.1$ and $\hat{\beta} = 0.2$). **(a)** Dimensional pathlines, with the replicative region also shown in green (width ≈ 0.19 mm at $t = 350$ hrs). The purple dashed line is from the experimental measurements. **(b)** Dimensional cell density at $t = 350$, where we have taken $\rho_0 = 1.1$ g/mL from Vulin et al. (2014).

our equations, similar to the work of Ward and King (1997). Another potential refinement would be to relax the simple assumption of a linear pressure–density relationship, and explore the effect of other non-linear functional forms. In particular, we might expect pressure to rise rapidly as the cell density increases towards some maximum packing density. All of these factors would tend to reduce the large variation in cell density observed in our model results in Fig. 9(b).

From an experimental perspective, it would be interesting to reproduce the experiment by Vulin et al. (2014) and incorporate fluorescence to track the position of tagged cells and trace the physical pathlines (Charvin et al., 2008). We then can use the pathlines to classify the quiescent and replicative region within the colony. This will provide a good experimental check with our theoretical results. Moreover, using fluorescence can also allow us to identify dead cells as shown in the supplementary material provided by Vulin et al. (2014). This will again be helpful in the validation of theoretical results if the model was extended to incorporate cell death.

In addition, as stated in the introduction, our model can be applicable to a range of other biological systems such as tissue and bone growth (Binder et al., 2008; Czarnecki et al., 2014). We assume the non-dimensional parameter values would be similar to the cylindrical yeast colonies as the cells would be non-motile and require nutrient to proliferate. However, we are unable to parameterise our model to other biological systems due to limitations in data availability. Hence, this could be a potential avenue for future research.

Declaration of competing interest

The authors declare that they have no known competing financial interests or personal relationships that could have appeared to influence the work reported in this paper.

Acknowledgements

KL and AJG acknowledge funding from the Australian Government through a Research Training Programme Scholarship. JEFG and BJB acknowledge funding from an Australian Research Council Discovery Project grant (DP230100406). The authors would like to thank Trent Mattner for useful discussions on the numerical computations.

References

Baker, R.E., Yates, C.A., Erban, R., 2010. From microscopic to macroscopic descriptions of cell migration on growing domains. Bull. Math. Biol. (ISSN: 1522-9602) 72 (3), 719–762. http://dx.doi.org/10.1007/s11538-009-9467-x.

Binder, B.J., Landman, K.A., Simpson, M.J., Mariani, M., Newgreen, D.F., 2008. Modeling proliferative tissue growth: a general approach and an avian case study. Physical Review E (ISSN: 1539-3755) 78 (3 Pt 1), 031912. http://dx.doi.org/10.1103/PhysRevE.78.031912.

Breward, C., Byrne, H., Lewis, C., 2002. The role of cell-cell interactions in a two-phase model for avascular tumour growth. J. Math. Biol. 45 (2), 125–152.

Byrne, H.M., Chaplain, M.A.J., 1995. Growth of nonnecrotic tumors in the presence and absence of inhibitors. Math. Biosci. (ISSN: 0025-5564) 130 (2), 151–181. http://dx.doi.org/10.1016/0025-5564(94)00117-3, URL https://www.sciencedirect.com/science/article/pii/0025556494001173.

Byrne, H., Chaplain, M., 1997. Free boundary value problems associated with the growth and development of multicellular spheroids. European J. Appl. Math. 8, http://dx.doi.org/10.1017/S0956792597003264.

Chaplain, M.A.J., 1996. Avascular growth, angiogenesis and vascular growth in solid tumours: The mathematical modelling of the stages of tumour development. Math. Comput. Modelling (ISSN: 0895-7177) 23 (6), 47–87. http://dx.doi.org/10.1016/0895-7177(96)00019-2, URL https://www.sciencedirect.com/science/article/pii/0895717796000192.

Charvin, G., Cross, F.R., Siggia, E.D., 2008. A microfluidic device for temporally controlled gene expression and long-term fluorescent imaging in unperturbed dividing yeast cells. PLoS One (ISSN: 1364-5021) 3 (1), e1468. http://dx.doi.org/10.1098/rspa.2019.0175, URL https://journals.plos.org/plosone/article?id=10.1371/journal.pone.0001468.

Crampin, E.J., Gaffney, E.A., Maini, P.K., 1999. Reaction and diffusion on growing domains: Scenarios for robust pattern formation. Bull. Math. Biol. (ISSN: 1522-9602) 61 (6), 1093–1120. http://dx.doi.org/10.1006/bulm.1999.0131.

Crank, J., 1987. Free and Moving Boundary Problems. Oxford University Press, Oxford, New York, ISBN: 978-0-19-853370-2.

Czarnecki, J., Jolivet, S., Blackmore, M., Lafdi, K., Tsonis, P., 2014. Cellular automata simulation of osteoblast growth on microfibrous-carbon-based scaffolds. Tissue Eng. http://dx.doi.org/10.1089/ten.TEA.2013.0387.

Deroulers, C., Aubert, M., Badoual, M., Grammaticos, B., 2009. Modeling tumor cell migration: From microscopic to macroscopic models. Phys. Rev. E 79 (3), 031917. http://dx.doi.org/10.1103/PhysRevE.79.031917, URL https://link.aps.org/doi/10.1103/PhysRevE.79.031917 Publisher: American Physical Society.

Driscoll, T.A., Braun, R.J., 2017. Fundamentals of Numerical Computation. SIAM, ISBN: 978-1-61197-508-6, Google-Books-ID W9JEDwAAQBAJ.

Gallo, A.J., Tronnolone, H., Green, J.E.F., Binder, B.J., 2021. Modelling uniaxial non-uniform yeast colony growth: Comparing an agent-based model and continuum approximations. J. Theoret. Biol. (ISSN: 1095-8541) 523, 110715. http://dx.doi.org/10.1016/j.jtbi.2021.110715.

Hecht, S., Vauchelet, N., 2017. Incompressible limit of a mechanical model for tissue growth with non-overlapping constraint. Commun. Math. Sci. (ISSN: 1539-6746)

15 (7), 1913–1932. http://dx.doi.org/10.4310/CMS.2017.v15.n7.a6, URL https://www.ncbi.nlm.nih.gov/pmc/articles/PMC5669502/.

Maini, P.K., McElwain, D.S., Leavesley, D., 2004. Travelling waves in a wound healing assay. Appl. Math. Lett. 17 (5), 575–580.

Neville, A.A., Matthews, P.C., Byrne, H.M., 2006. Interactions between pattern formation and domain growth. Bull. Math. Biol. (ISSN: 0092-8240) 68 (8), 1975–2003. http://dx.doi.org/10.1007/s11538-006-9060-5.

Painter, K.J., 2009. Continuous models for cell migration in tissues and applications to cell sorting via differential chemotaxis. Bull. Math. Biol. (ISSN: 0092-8240) http://dx.doi.org/10.1007/s11538-009-9396-8, Publisher: New York : Springer-Verlag.

Sadiku, M.N.O., Obiozor, C.N., 2000. A Simple Introduction to the Method of Lines. Int. J. Electr. Eng. Educ. (ISSN: 0020-7209) 37 (3), 282–296. http://dx.doi.org/10.7227/IJEEE.37.3.8, Publisher: SAGE Publications Ltd STM.

Tam, A., Green, J.E.F., Balasuriya, S., Tek, E.L., Gardner, J.M., Sundstrom, J.F., Jiranek, V., Binder, B.J., 2019. A thin-film extensional flow model for biofilm expansion by sliding motility. Proc. R. Soc. Lond. Ser. A Math. Phys. Eng. Sci. (ISSN: 1364-5021) 475 (2229), 20190175. http://dx.doi.org/10.1098/rspa.2019.0175.

Vulin, C., Di Meglio, J.-M., Lindner, A.B., Daerr, A., Murray, A., Hersen, P., 2014. Growing yeast into cylindrical colonies. Biophys. J. (ISSN: 1542-0086) 106 (10), 2214–2221. http://dx.doi.org/10.1016/j.bpj.2014.02.040.

Ward, J.P., King, J.R., 1997. Mathematical modelling of avascular-tumour growth. Math. Med. Biol. (ISSN: 1477-8599) 14 (1), 39–69. http://dx.doi.org/10.1093/imammb/14.1.39.

Yates, C.A., Baker, R.E., Erban, R., Maini, P.K., 2012. Going from microscopic to macroscopic on nonuniform growing domains. Phys. Rev. E 86 (2), 021921.